THE JOURNAL OF BIOLOGICAL CHEMISTRY
Vol. 276, No. 20, Issue of May 18, pp. 17387–17394, 2001
Printed in U.S.A.

Molecular Cloning and Characterization of a Novel $(Na^+,K^+)/H^+$ Exchanger Localized to the *trans*-Golgi Network*

Received for publication, February 12, 2001
Published, JBC Papers in Press, February 26, 2001, DOI 10.1074/jbc.M101319200

Masayuki Numata and John Orlowski‡

From the Department of Physiology, McGill University, Montréal, Québec H3G 1Y6, Canada

The luminal pH of organelles along the secretory and endocytic pathways of mammalian cells is acidic and tightly regulated, with the $[H^+]$ varying up to 100-fold between compartments. Steady-state organellar pH is thought to reflect a balance between the rates of H^+ pumping by the vacuolar-type H^+-ATPase and H^+ efflux through ill-defined pathways. Here, we describe the cloning of a novel gene (*NHE7*) in humans that is homologous to Na^+/H^+ exchangers, is ubiquitously expressed, and localizes predominantly to the *trans*-Golgi network. Significantly, NHE7 mediates the influx of Na^+ or K^+ in exchange for H^+. The activity of NHE7 was also found to be relatively insensitive to inhibition by amiloride but could be antagonized by the analogue benzamil and the unrelated compound quinine. Thus, NHE7 displays unique functional and pharmacological properties and may play an important role in maintaining cation homeostasis of this important organelle.

The luminal ionic composition of many, if not all, intracellular compartments differs from the surrounding cytoplasm and is an important determinant of their function. The establishment of this differential composition is achieved through the concerted actions of distinct integral membrane ion carriers, including pumps, channels, and transporters. For example, alkalinization of the mitochondrial matrix, driven by the respiratory chain, contributes to the inner membrane H^+ gradient used to drive ATP synthesis (1) and, indirectly, to extrude matrix Ca^{2+} through the functional coupling of Na^+/H^+ and Na^+/Ca^{2+} antiport pathways (2–4).

By contrast, organelles of the secretory and endocytic pathways are distinguished by their luminal acidity, which is generated by the activity of an electrogenic vacuolar-type H^+-ATPase (V-ATPase)[1] (5, 6). Progressive acidification of vesicles in the endocytic pathway (early and late endosomes, pH ~6.5 → lysosomes, pH ~4.5) is essential for the redistribution and degradation of internalized membrane proteins, such as ligand-receptor complexes and fluid-phase solutes (5, 7). Likewise, increasing luminal acidification of compartments of the exocytic pathway (endoplasmic reticulum, pH ~7.0 → Golgi complex, pH ~6.5 → *trans*-Golgi network (TGN), pH ~6.0 → secretory vesicles, pH ~5.0) is important for proper post-translational processing and sorting of newly synthesized proteins (5, 8, 9).

At present, little is known about the mechanisms controlling the steady-state $[H^+]$ within the lumen of different endomembrane compartments. Although distinct isoforms of some of the V-ATPase subunits have been reported in different tissues (10, 11) or specialized cell types (12), there is no clear evidence that the V-ATPase functions differently in particular organelles within a single mammalian cell (although this may not be the case in yeast (13)). It has been suggested that because the pump is electrogenic, its activity could be influenced by the membrane potential and by the availability of permeant counterions such as chloride and potassium (14). However, in the case of the Golgi complex, the endogenous counterion conductances were found to exceed the rate of H^+ pumping at the steady state, implying that the electrical potential across the membrane is negligible and therefore not a defining factor in setting organellar pH (15–17). In addition, despite extensive work, differential control of V-ATPase activity by hormones or other factors has not been found along the endo- or exocytic pathways. Rather, the luminal $[H^+]$ is thought to be regulated by a complex interplay between the V-ATPase and unidentified leak pathways for protons, based on the rapid dissipation of the transmembrane proton chemical gradient (ΔpH) observed after inhibiting the V-ATPase with macrolide antibiotics (15, 16, 18). A component of this H^+ leak in the Golgi complex was recently identified as a Zn^{2+}-inhibitable H^+ conductance (17) but could not fully account for H^+ turnover. Nevertheless, it highlights the H^+ leak as a key determinant of organellar pH and emphasizes the need to identify the molecular components of this pathway which, in addition to putative H^+ channels, could conceivably involve H^+ proton-coupled cotransporters or exchangers.

In this study, we describe the cloning and functional characterization of a unique monovalent cation/proton exchanger that localizes predominantly to the *trans*-Golgi network and suggests a novel molecular mechanism for controlling the luminal cation composition of this important organelle.

EXPERIMENTAL PROCEDURES

Molecular Cloning— Two overlapping human ESTs with homology to known mammalian Na^+/H^+ exchangers were identified in GenBank™ (accession number AA279477 and AA648924) and obtained from Genome Systems Inc. (St. Louis, MO). Examination of the cDNA sequences (designated as NHE7) indicated that they were missing coding information at the 5′ and 3′ regions (*i.e.* start and stop codons, respectively). To obtain the complete nucleotide sequence, we isolated cDNA fragments corresponding to the missing 3′-end (amino acids 624–725) from a human bone marrow cDNA library using rapid amplification of cDNA ends methodology (19). However, we were unable to clone the

* This work was supported by the Canadian Institutes for Health Research. The costs of publication of this article were defrayed in part by the payment of page charges. This article must therefore be hereby marked "*advertisement*" in accordance with 18 U.S.C. Section 1734 solely to indicate this fact.

‡ To whom correspondence should be addressed: Dept. of Physiology, McGill University, McIntyre Medical Sciences Bldg., 3655 Promenade Sir-William-Osler, Montreal, Quebec H3G 1Y6, Canada. Tel.: 514-398-8335; Fax: 514-398-7452; E-mail: orlowski@med.mcgill.ca.

[1] The abbreviations used are: V-ATPase, vacuolar-type H^+-ATPase; TGN, *trans*-Golgi network; PCR, polymerase chain reaction; HA, hemagglutinin; PBS, phosphate-buffered saline; PAGE, polyacrylamide gel electrophoresis; FITC, fluorescein isothiocyanate; EcR, ecdysone-activated receptor; CHO, Chinese hamster ovary; GFP, green fluorescent protein; CCCP, carbonyl cyanide *m*-chlorophenylhydrazone; COX IV, cytochrome oxidase subunit IV.

5′-end of the cDNA using this approach. While this work was in progress, the sequences covering the 3′-end of the cDNA, but not the 5′-end, were found to match nucleotide sequences present in a human genomic fragment (GenBank™ accession number AL022165) that mapped to chromosome Xp11. To determine the missing 5′-sequence, we screened a human X chromosome library (20) available from the American Tissue Culture Collection (ATCC) using a 123-base pair polymerase chain reaction (PCR)-generated fragment corresponding to the most 5′-end of one of the EST clones (GenBank™ accession number AA648924). Four overlapping positive clones were isolated by screening 4×10^4 independent clones from the library. The largest insert was subcloned into a plasmid vector, and the missing sequence (the first 53 amino acids), in addition to downstream sequence that precisely overlapped the 5′-end of the EST clone, was found to reside within a single predicted exon. The presence of this sequence in the NHE7 transcript was verified by reverse transcriptase-polymerase chain reaction (PCR) using human bone marrow and skeletal muscle poly(A^+) RNA. The predicted translation initiation codon is preceded by a purine nucleotide in position −3 and downstream contains a purine at position +4, placing it in a good context for initiation by eukaryotic ribosomes, as defined by Kozak (21). In addition, the apparent translation initiation site is also preceded by an in-frame stop codon at nucleotide position −336. The 5′-end of the NHE7 cDNA sequence was subsequently found to match uncharacterized genomic sequences that map to chromosome Xp11.1–11.4 (GenBank™ accession number AL050307). The full-length cDNA was reconstituted by PCR and the integrity of the construct was verified by DNA sequencing. The complete cDNA sequence was deposited in GenBank™ (accession number AF298591).

RNA Blotting—Human poly(A^+) mRNA Northern and Master dot blots (CLONTECH) were hybridized with a 0.2-kilobase pair PCR fragment generated from the 3′-end of NHE7 that shares minimal sequence identity with other NHE isoforms. The PCR probe was agarose gel-purified and radiolabeled with [α-^{32}P]dCTP by the random primer method. Hybridization was done at 65 °C in Church buffer containing 7% SDS, 0.5 M sodium phosphate, pH 7.2, 1% bovine serum albumin and 2 mM EDTA overnight. The blots were washed twice in 2× SSC, 0.05% SDS at room temperature for 30 min each, followed by three higher stringency washes in 0.1× SSC containing 0.1% SDS at 68 °C for 30 min each. The radioactive signals were analyzed by a PhosphorImager (Molecular Dynamics, Sunnyvale, CA).

Stable Transfection and Expression of NHE7—The full-length NHE7 cDNA was engineered to include the influenza virus hemagglutinin (HA) epitope, YPYDVPDYAS (preceded by a single G amino acid linker inserted to create peptide flexibility), at the very C-terminal end (called $NHE7_{HA}$) using PCR mutagenesis to allow for immunological detection of the protein. In a separate construct, an HA epitope was also inserted at an internal site, Leu^{488} ($NHE7_{488HA}$). The $NHE7_{HA}$ construct was subcloned into the ecdysone-inducible expression vector pIND (Invitrogen) and transfected into Chinese hamster ovary cells that constitutively express an ecdysone-activated receptor (EcR-CHO cells; Invitrogen). Cells stably expressing both $NHE7_{HA}$ and EcR were selected in α-minimum Eagle's medium supplemented with 10% fetal bovine serum, 100 units/ml penicillin, 100 μg/ml streptomycin, 25 mM $NaHCO_3$, pH 7.4, and containing 600 μg/ml G418 and 250 μg/ml zeocin. The cells were maintained in an humidified atmosphere of 95% air and 5% CO_2 at 37 °C. Single colonies were isolated, and the regulated expression of $NHE7_{HA}$ was verified by Western blotting and immunofluorescence microscopy in the presence of increasing concentrations (0–10 μM) of the ecdysone analogue, ponasterone A, for 24 h.

Western Blotting—Cells were washed three times with ice-cold PBS and then lysed with triple detergent buffer (150 mM NaCl, 0.1% SDS, 1% IGEPAL CA-630, 0.5% sodium deoxycholate and 50 mM Tris-HCl, pH 8.0) supplemented with proteinase inhibitor mixture (Roche Molecular Biochemicals) for 5–10 min on ice. Cell lysates were spun at 12,000 × *g* for 5 min to remove insoluble cell debris, separated in a 7.5% SDS-PAGE, and then transferred to a polyvinylidene difluoride membrane (Amersham Pharmacia Biotech). The blot was briefly rinsed with PBS, blocked with 5% non-fat skim milk in PBS for 1 h, and then incubated with mouse monoclonal antibodies against either the HA epitope (Babco, Berkley, CA) at a 1/5,000 dilution or cytochrome oxidase subunit IV (COX IV) (Molecular Probes, Eugene, OR) at a 1/200 dilution. After extensive washes with PBS containing 0.1% Tween 20, the blot was incubated with goat anti-mouse IgG second antibody conjugated with horseradish peroxidase (Jackson Laboratory, Bar Harbor, ME) at a dilution of 1/20,000. Green fluorescent protein (GFP) was detected with a rabbit polyclonal anti-GFP antibody (1/100 dilution) (CLONTECH) followed by incubation with a mouse anti-rabbit IgG secondary antibody conjugated with horseradish peroxidase (New England Biolabs) at a dilution of 1/3000. Immunoreactive bands were detected by enhanced chemiluminescence (Amersham Pharmacia Biotech) and exposed to an x-ray film.

Immunofluorescence Confocal Microscopy—For immunofluorescence confocal microscopy studies, $NHE7_{HA}$-transfected EcR-CHO cells were grown on glass coverslips and incubated in the presence of 5 μM ponasterone A for 24 h. The cells were subsequently fixed with 2% paraformaldehyde/PBS for 20 min, permeabilized in 0.1% Triton X-100, blocked with 5% non-fat skim milk in PBS for another 20 min, and then incubated with monoclonal anti-HA antibody at a dilution of 1/1000 for 1 h. After extensive washing, cells were incubated with Cy3-conjugated goat anti-mouse IgG secondary antibody (1/800 dilution) for 1 h. For double labeling experiments with polyclonal antibodies to organelle-specific markers, the signals were visualized using Oregon Green or FITC-conjugated donkey anti-rabbit IgG (Molecular Probes and Jackson Laboratory, respectively). In the case of the TGN marker, a mammalian expression vector containing the CD25-TGN38 chimeric gene (22) was transiently transfected into the cells, and the protein was visualized by FITC-conjugated anti-CD25 antibody (Serotec, Raleigh, NC). The coverslips were washed, mounted onto glass slides, and analyzed by confocal laser scanning microscopy using a Zeiss inverted microscope. Images were processed using Adobe® Photoshop™ version 5.5 and CorelDraw™ version 8.0.

Measurements of Organellar $^{22}Na^+$ and $^{86}Rb^+$ Influx—Rates of $^{22}Na^+$ and $^{86}Rb^+$ influx into endomembrane structures were measured in control and ponasterone A-induced (10 μM; 24-h treatment) NHE7-transfected EcR-CHO cells that were permeabilized with saponin (50 μg/ml) in K^+-rich buffer (in mM: 140 KCl, 2 $CaCl_2$, 2 EGTA, 1 $MgCl_2$, 2 Mg^{2+}-ATP, 20 HEPES, pH 7.2) at 20 °C for 4.5 min, followed by multiple washes. Influx measurements were conducted in choline chloride-rich buffer (in mM: 140 choline chloride, 2 $CaCl_2$, 1 $MgCl_2$, 2 Mg^{2+}-ATP, 1 EGTA, 10 HEPES-Tris, pH 7.8). Following a 5-min uptake period, the cells were quickly washed three times with ice-cold stop buffer (in mM: 140 NaCl (for $^{22}Na^+$ influx) or 140 KCl (for $^{86}Rb^+$ influx), 2 $CaCl_2$, 1 $MgCl_2$, 10 HEPES, pH 5.5). To extract the radiolabel, the monolayers were solubilized with 0.5 N NaOH and neutralized with 0.5 N HCl, and the pooled extracts were assayed by liquid scintillation spectroscopy. Protein content was determined using the Bio-Rad DC protein assay kit according to the manufacturer's protocol. Each experiment was repeated at least three times.

RESULTS AND DISCUSSION

A search of the GenBank™ data base for candidate genes homologous to known mammalian Na^+/H^+ exchangers (*i.e.* NHE1-NHE6) (23–25) identified two novel overlapping expressed sequence tags from human (GenBank™ accession numbers AA279477 and AA648924). These shared highest sequence identity to the mitochondrion-targeted NHE6 isoform rather than to the plasmalemmal NHEs (*i.e.* NHE1–5), suggesting that the gene product (which we designate as NHE7) may also reside in an intracellular compartment. Examination of the sequences of the putative NHE7 cDNAs indicated that they lacked coding information at the 5′- and 3′-ends. To obtain the complete nucleotide sequence, we sequenced cDNAs isolated from a single-stranded cDNA library that had been generated from human bone marrow poly(A^+) mRNA using rapid amplification of cDNA ends methodology and genomic fragments cloned from a human λ phage library (for details, see "Experimental Procedures").

The deduced primary sequence of NHE7 is composed of 725 amino acids (calculated M_r = 80,132) and exhibits high amino acid identity (~70%) to NHE6 (Fig. 1*A*) but low similarity (~25%) to other NHEs. Based on hydropathy plot analysis, NHE7 is predicted to contain 12 α-helical hydrophobic membrane-spanning (M) segments in the N terminus followed by a hydrophilic cytoplasmic tail at the C terminus, similar to other NHEs (Fig. 1*B*). Recent biochemical and molecular topological studies of the NHE1 isoform partially support this structural model (26, 27), although some notable changes in the arrangement of the C-terminal transmembrane segments have been proposed (27), namely the predicted M10 segment was suggested to reside within the lipid bilayer (the predicted M11 was renamed M10), whereas the last extracellular loop was found to form an

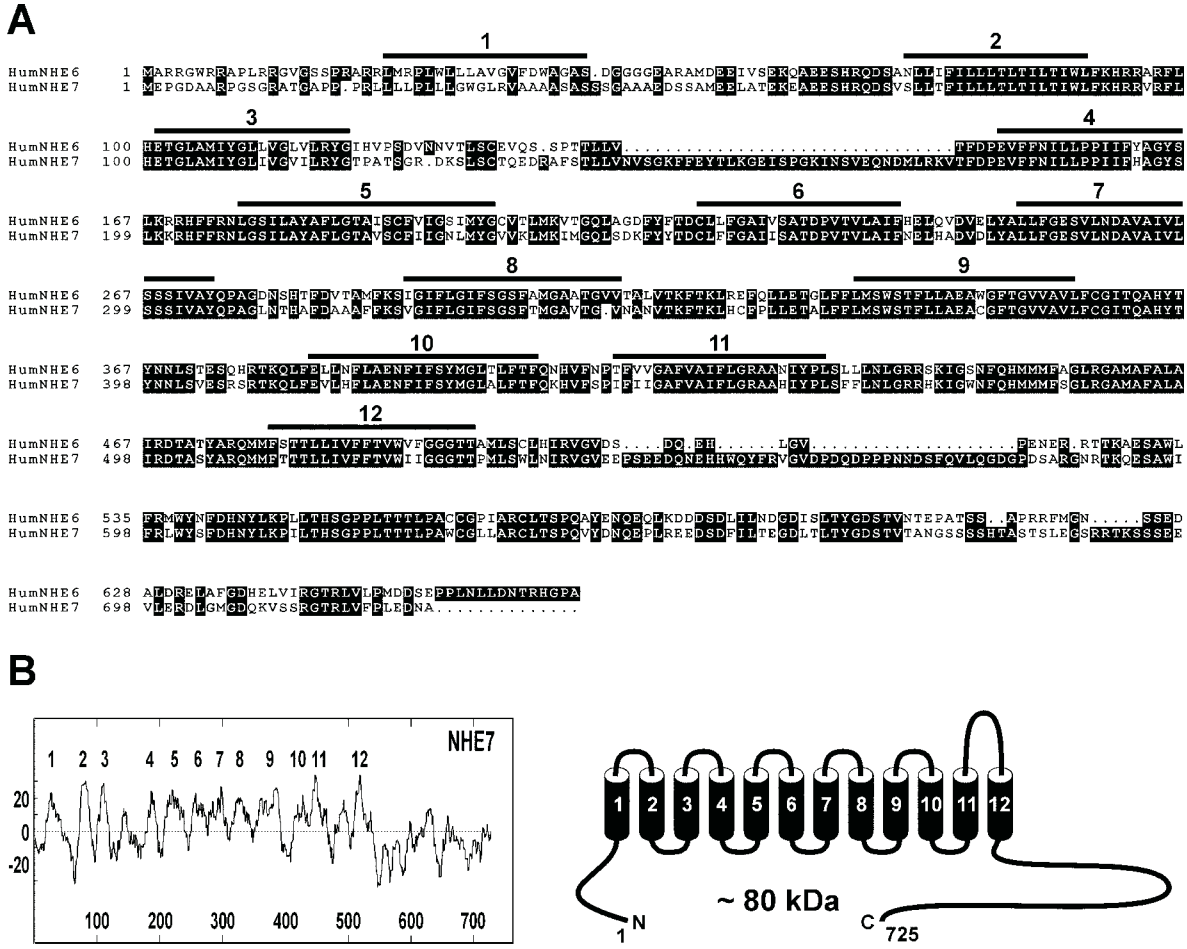

FIG. 1. **Primary structure and predicted membrane topology of the human NHE7 isoform.** *A,* amino acid sequences of human NHE6 (HumNHE6) and human NHE7 (HumNHE7) (GenBank™ accession numbers D87743/AF030409 and AF298591, respectively) were aligned using the ClustalW algorithm. Gaps (indicated by *periods*) were introduced in the sequence to maintain the alignment. Positions containing identical residues are *shaded* in *black,* and conservative amino acid differences are *shaded* in *gray*. Predicted membrane-spanning segments are numbered 1–12 and indicated by an *overline. B*, a hydrophobicity plot determined by the algorithm of Kyte and Doolittle (window of 11 amino acids) (63) and corresponding model of the transmembrane organization of the NHE7 protein are shown.

intracellular loop, a new transmembrane segment (M11), and an extracellular loop. Unlike NHE1, a recent report has suggested that a part of the cytoplasmic C terminus of the NHE3 isoform may reside at the exoplasmic surface (28). Whether these structural features of the plasmalemmal NHEs also apply to the more distantly related organellar NHEs remains to be determined.

Northern blot analysis of selected human tissues using an isoform-specific cDNA probe from the 3′-coding region revealed three NHE7 mRNA transcripts of ~9.5, 7.5, and 3.0 kilobases in length under high stringency hybridization conditions (Fig. 2*A*). More extensive RNA dot blot analyses of human tissues showed that the gene is expressed ubiquitously (Fig. 2*B*) but most prominently in certain regions of the brain (putamen and occipital lobe), skeletal muscle, and secretory tissues (prostate, stomach, pancreas, pituitary gland, adrenal gland, thyroid gland, salivary gland, and mammary gland). Each of the mRNAs is of sufficient length to contain the entire coding region, which could result from differential processing of the untranslated regions or alternative-splicing of a single gene product. The former is favored since attempts to identify alternatively spliced variants within the coding region by reverse transcriptase-PCR were unsuccessful. Alternatively, certain transcript(s) may represent other closely related genes that have yet to be characterized. This broad pattern of expression is consistent with NHE7 serving a "housekeeping" function.

To facilitate expression and localization of NHE7, we inserted an influenza virus hemagglutinin (HA) epitope at the extreme C terminus ($NHE7_{HA}$). The full-length $NHE7_{HA}$ cDNA was subcloned into the ecdysone-inducible expression vector pIND and stably transfected into Chinese hamster ovary cells engineered to express constitutively an ecdysone-activable receptor (EcR-CHO cells). Regulated expression of $NHE7_{HA}$ was verified by incubating isolated $NHE7_{HA}$-transfected EcR-CHO cell colonies in the presence of increasing concentrations of ponasterone A, an analogue of ecdysone. As shown in Fig. 3, ponasterone A induced a dose-dependent increase in the expression of $NHE7_{HA}$, which migrated as two broad bands of ~180 and 80 kDa by SDS-PAGE analysis. The faster migrating band corresponds to the predicted size of the protein. The larger band may represent the formation of a homodimer that is modestly stable in SDS, as has been reported for NHE1 and NHE3 (29). The bands are diffuse, suggesting the presence of glycosylation or other post-translational modifications. Consistent with this possibility, the N terminus contains putative *N*-linked glycosylation sites in the predicted extracellular loop between M3 and M4 (Asn^{145}-Val-Ser) and between M9 and M10 (Asn^{400}-Leu-Ser). Although the latter site is highly conserved in eukaryotic NHEs, it does not appear to be glycosylated in other mammalian NHE isoforms (*i.e.* NHE1, NHE2, and NHE3) (30–32) and therefore is unlikely to be modified in NHE7.

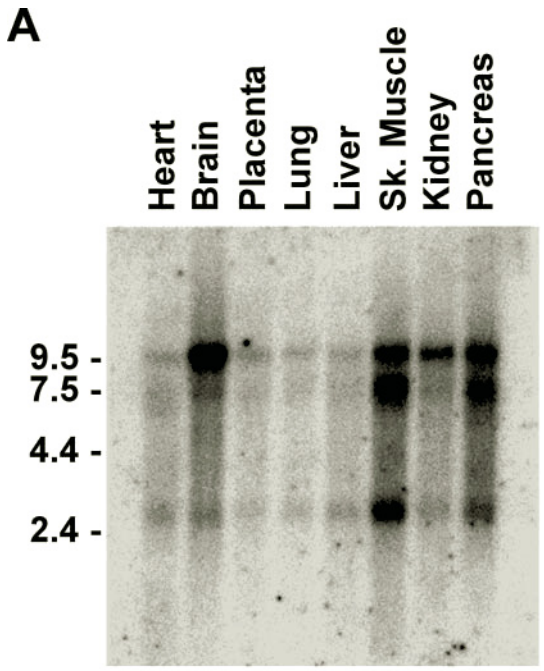

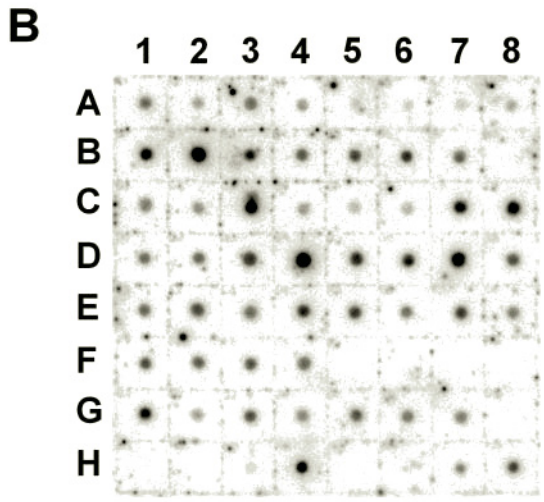

A	whole brain	amygdala	caudate nucleus	cere-bellum	cerebral cortex	frontal lobe	hippo-campus	medulla oblongata
B	occipital lobe	putamen	substantia nigra	temporal lobe	thalamus	nucleus accumbeus	spinal cord	
C	heart	aorta	skeletal muscle	colon	bladder	uterus	prostate	stomach
D	testis	ovary	pancreas	pituitary gland	adrenal gland	thyroid gland	salivary gland	mammary gland
E	kidney	liver	small intestine	spleen	thymus	peripheral leukocytes	lymph node	bone marrow
F	appendix	lung	trachea	placenta				
G	fetal brain	fetal heart	fetal kidney	fetal liver	fetal spleen	fetal thymus	fetal lung	
H	yeast total RNA 100 ng	yeast tRNA 100 ng	*E. coli* rRNA 100 ng	*E. coli* DNA 100 ng	Poly r(A) 100 ng	human C_{ot} 1 DNA 100 ng	human DNA 100 ng	human DNA 500 ng

FIG. 2. **Expression of NHE7 mRNA in human tissues.** A human tissue poly(A^+) RNA Northern blot (2 μg of RNA *per* lane) (*A*) and a human poly(A^+) RNA Master^{TM} dot blot (CLONTECH) (*B*) were hybridized with an isoform-specific ^{32}P-labeled NHE7 cDNA probe (0.2 kilobase pairs) under high stringency conditions. The radioactive signals were detected using a PhosphorImager (Molecular Dynamics). The positions and sizes (in kilobases) of the RNA markers in *A* are shown on the *left*.

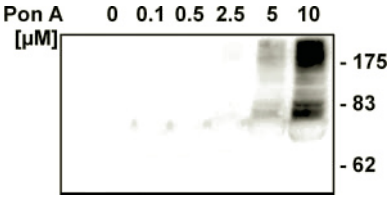

FIG. 3. **Ecdysone-inducible expression of recombinant $NHE7_{HA}$ in stably transfected EcR-CHO cells.** Cell lysates were prepared from an EcR-CHO cell line stably transfected with $NHE7_{HA}$ following incubation with increasing concentrations (0–10 μM) of the ecdysone analogue, ponasterone A, for 24 h. Fifty μg of each cell lysate were subjected to 7.5% SDS-PAGE and immunoblotted with an anti-HA monoclonal antibody. Molecular weight markers are shown on the *right*.

To define the subcellular distribution of $NHE7_{HA}$, $NHE7_{HA}$-transfected EcR-CHO cells were treated with a submaximal concentration of ponasterone A (5 μM) for 24 h and then examined using immunofluorescence confocal microscopy. Typically under these conditions, ~50% of the cells in different stable transfectants were found to express detectable levels of $NHE7_{HA}$. The partial penetrance of $NHE7_{HA}$ expression upon ponasterone A induction was also observed in individual secondary and tertiary isolates obtained by dilution subcloning. The cellular basis for this limited expression pattern is unclear but may relate to the site of genomic integration of the ecdysone receptor gene and/or the stage of the cell cycle.

Representative dual labeling experiments revealed that $NHE7_{HA}$ accumulates predominantly in a juxtanuclear compartment that was closely apposed but somewhat broader than the compact structure labeled by an antibody against α-mannosidase II, an established marker of the medial and *trans*-cisternae of the Golgi (Fig. 4, *A–C*) (33). Transient expression of two additional constructs, one containing an internal HA-tag inserted at position Leu^{488} and the other containing a C-terminal c-Myc epitope, gave similar results, suggesting that the protein distribution is not influenced by the position or sequence of the tag. The pattern was clearly distinct from those observed with antibodies that recognize specific markers of the endoplasmic reticulum (calnexin), lysosomes (cathepsin B and D), or mitochondria (mito-green fluorescent protein (mito-GFP) (34) and COX IV) (data not shown). $NHE7_{HA}$ also did not appear to accumulate at the cell surface nor was it able to functionally complement a mutant strain of CHO cells lacking plasmalemmal NHE activity (35) (data not shown).

The comparatively broader immunofluorescence signal of $NHE7_{HA}$ relative to that of α-mannosidase II suggested that it may be present in compartments distal to the Golgi cisternae, such as the TGN and possibly endosomes. To define further NHE7 compartmentation, cells were treated with different pharmacological agents that are known to affect the Golgi, TGN, and endosomes differentially. The fungal metabolite brefeldin A causes the disassembly of the Golgi apparatus by promoting the retrograde absorption and dispersion of Golgi cisternae resident proteins into the endoplasmic reticulum (36, 37), thereby creating a mixed endoplasmic reticulum/Golgi compartment. It concomitantly induces the coalescence of the TGN with early endosomes into a dense juxtanuclear tubulovesicular structure (38, 39). As shown in Fig. 4, pretreatment of cells with brefeldin A (5 μg/ml for 2 h at 37 °C) dispersed the immunofluorescence signal of α-mannosidase II (Fig. 4, *E* and *F*) into a reticular pattern, whereas that of $NHE7_{HA}$ (Fig. 4, *D* and *F*) was largely retained in a compact juxtanuclear complex, with a minor fraction diffusely distributed throughout the cell. These data suggest that $NHE7_{HA}$ is concentrated primarily in the TGN/early endosomal structure. The location of the TGN was defined by transiently transfecting the cells with an ex-

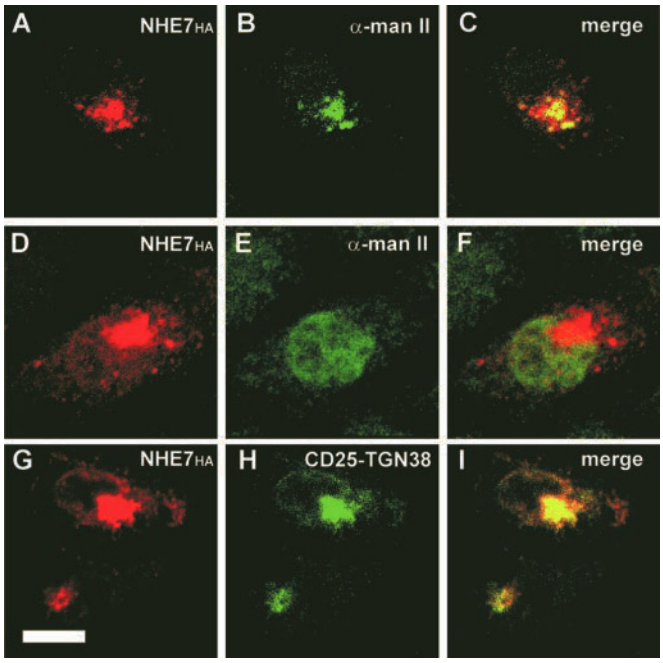

FIG. 4. **Subcellular localization of human NHE7$_{HA}$ in stably transfected EcR-CHO cells.** To define the subcellular distribution of NHE7$_{HA}$, EcR-CHO cells were treated with a suboptimal concentration of ponasterone A (5 μM) for 24 h. Subsequently, the cells were incubated in the absence (*A–C*) or presence (*D–F*) of 5 μg/ml brefeldin A for 2 h at 37 °C. The cells were then fixed, permeabilized, and dual labeled with a mouse monoclonal antibody to the HA epitope (NHE7$_{HA}$) followed by Cy3-conjugated secondary antibody (*A, D,* and *G*) and a rabbit polyclonal antibody to the endogenous Golgi cisternae marker α-mannosidase II (*α-man II*) followed by Oregon Green-conjugated secondary antibody (*B* and *E*). In certain experiments, NHE7-induced cells were transiently transfected (24-h period) with the TGN marker CD25-TGN38, and the chimeric protein was detected by FITC-conjugated anti-CD25 antibody (*H*). Composite images of the dual labels are shown in *C, F,* and *I*. *Scale bar*, 10 μm.

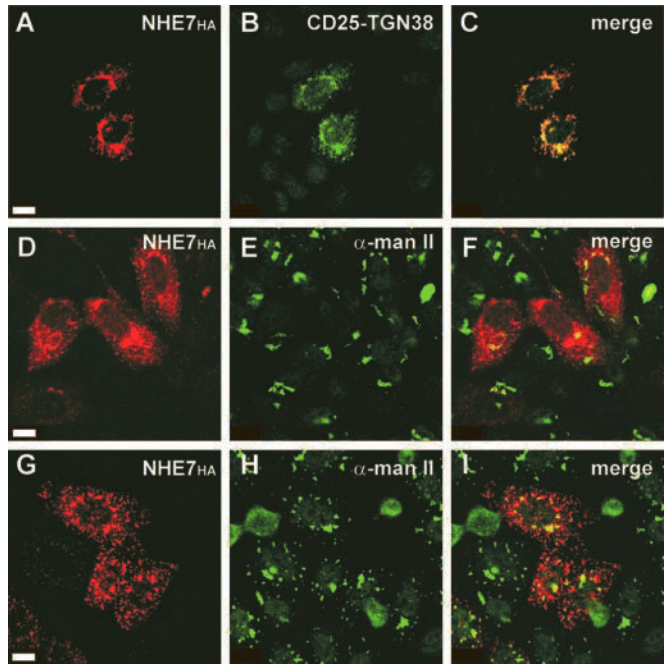

FIG. 5. **Effect of nocodazole on the subcellular distribution of NHE7$_{HA}$.** Expression of NHE7$_{HA}$ was induced in EcR-CHO cells by 5 μM ponasterone A for 24 h. In certain experiments, NHE7-induced cells were transiently transfected (24-h period) with the TGN marker CD25-TGN38. Subsequently, the cells were incubated in the presence of 10 μM nocodazole for 1 h (*A–F*) or 4 h (*G–I*) at 37 °C. The cells were then fixed, permeabilized, and dual labeled with a mouse monoclonal antibody to the HA epitope (NHE7$_{HA}$) followed by Cy3-conjugated secondary antibody (*A, D,* and *G*), and a FITC-conjugated anti-CD25 antibody (*B*) or rabbit polyclonal antibody to the endogenous Golgi cisternae marker α-mannosidase II (*α-man II*) followed by Oregon Green-conjugated secondary antibody (*E* and *H*). Composite images of the dual labels are shown in *C, F,* and *I*. *Scale bar*, 10 μm.

pression vector containing the chimeric gene *CD25-TGN38*. This chimera, which is composed of the extracellular domain of the α-chain of the interleukin-2 receptor linked to the transmembrane and cytosolic domains of TGN38, has been shown to accumulate in the TGN and can be readily labeled with commercially available FITC-conjugated CD25 antibodies (15, 22). As shown in Fig. 4, *G–I*, the distribution of NHE7$_{HA}$ precisely overlapped that of CD25-TGN38, suggesting it is predominantly in the TGN.

To establish further the compartmentation of NHE7$_{HA}$, cells were treated with the microtubule-disrupting agent nocodazole, which causes initial dispersion of the TGN and endosomes (early event), followed by the redistribution of the Golgi cisternae (late event), into discrete vesicular compartments throughout the cytoplasm (37, 40). As shown in Fig. 5, *A–C*, acute treatment with nocodazole (10 μM for 1 h) caused the TGN marker CD25-TGN38 to scatter in a pattern precisely matching that of NHE7$_{HA}$, whereas the distribution of α-mannosidase II in the Golgi cisternae remained relatively compact (Fig. 5, *D–F*). However, after a 4-h exposure to nocodazole, the α-mannosidase II signal also dispersed in a pattern that was distinct from, but partially overlapping, that of NHE7$_{HA}$ (Fig. 5, *G–I*). In similarly treated cells, endomembrane vesicles containing NHE7$_{HA}$ also did not precisely colocalize with those containing transiently transfected, Myc-tagged NHE3, which is known to accumulate at the cell surface but also in endocytic or recycling endosomal vesicles of CHO cells (41) (data not shown). Taken together, these data suggest that some NHE7 may be present in the Golgi cisternae but most is situated in the TGN.

It is noteworthy that NHE7, unlike the closely related NHE6 isoform, lacks an obvious mitochondrial targeting sequence at its N terminus (*i.e.* ~20–60 amino acids with abundant basic residues that are predicted to form an amphipathic α-helix) (42). However, NHE7 does contain putative motifs for Golgi targeting and/or retention, including a unique Ser/Thr-phosphorylatable acidic cluster (^{542}EEPSEEDQNE^{551}) (43) and a tyrosine-based sequence (^{556}YFRV^{559}) (44). Differential localization of NHE7 and NHE6 was further demonstrated biochemically by subcellular fractionation of the endomembrane compartments using differential centrifugation and Western blotting with antibodies that recognize either endogenous or ectopically expressed organelle-specific markers. As shown in Fig. 6, NHE7$_{HA}$ was associated with the microsomal enriched membrane fraction (P100 pellet) isolated from cells that were also transiently transfected with Golgi-targeted green fluorescent protein (g-GFP), a convenient marker for this fraction (34). By contrast, NHE6$_{HA}$ (also stably expressed under the control of the ecdysone-inducible promoter in another CHO cell line) accumulated in the mitochondrion-enriched fraction (P10 pellet), as defined molecularly by the presence of the mitochondrion-specific marker COX IV. Neither NHE7$_{HA}$ nor NHE6$_{HA}$ was present in the soluble fractions (S100) isolated from cells that were transiently transfected with an expression plasmid containing cytoplasmic GFP (c-GFP) as a marker (34).

To assess NHE7$_{HA}$ activity, we adapted procedures that had been used previously for measuring $^{45}Ca^{2+}$ uptake and release from the Golgi (45). The plasma membrane was selectively permeabilized with saponin, and $^{22}Na^{+}$ uptake into intact endomembrane compartments was compared with and without ponasterone A-induced overexpression of NHE7$_{HA}$. Prelimi-

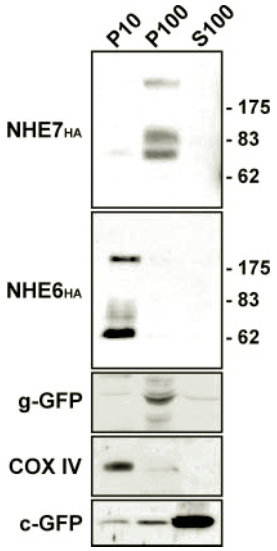

FIG. 6. **Subcellular fractionation and immunoblot analysis of $NHE7_{HA}$ expressed in EcR-CHO cells.** Expression of $NHE7_{HA}$ was induced by 5 μM ponasterone A for 16 h. Cell lysates were prepared by mild disruption through a 26.5-gauge needle in 250 mM sucrose, 10 mM HEPES-NaOH, 1 mM EDTA, pH 7.5, in the presence of a proteinase inhibitor mixture (Roche Molecular Biochemicals). Nuclei and insoluble cell debris were sedimented by centrifugation at 500 $\times$ *g*. The mitochondrial and microsomal fractions were obtained from the supernatant by sequential centrifugation at 10,000 and 100,000 $\times$ *g*, respectively, and the resulting pellets were isolated and designated *P10* and *P100*. Each fractionated pellet was resuspended in an identical volume of lysis buffer. The final supernatant fraction (*S100*) represented the cytosolic fraction. For comparison, parallel subcellular fractionation experiments were conducted using cell lysates prepared from an EcR-CHO cell line stably transfected with human NHE6 tagged with an HA epitope at its C terminus ($NHE6_{HA}$) following exposure to 5 μM ponasterone A for 24 h. $NHE6_{HA}$ is found in the P10 fraction, consistent with its known accumulation in mitochondria. Additional controls include $NHE7_{HA}$-expressing cells transiently transfected with an expression vector containing either a cDNA chimeric construct composed of the signal peptide from the Golgi protein human β-1,4-galactosyltransferase linked to GFP (g-GFP) (34) or GFP lacking a membrane targeting signal (cytoplasmic GFP or c-GFP). Equivalent volumes of each fraction were then subjected to 10% SDS-PAGE and immunoblotted with antibodies to HA, GFP, or COX IV.

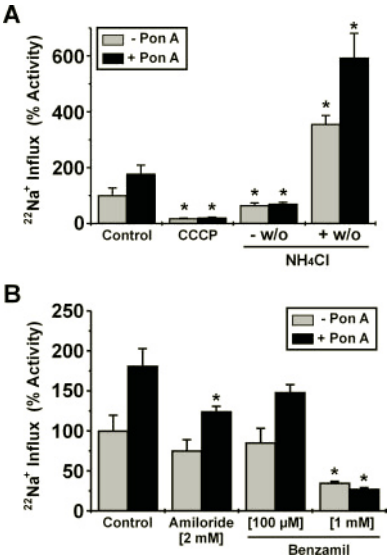

FIG. 7. **Measurements of H^+-dependent $^{22}Na^+$ influx into endomembrane compartments of $NHE7_{HA}$-transfected EcR-CHO cells.** $NHE7_{HA}$-transfected EcR-CHO cells were grown to confluence in 24-well plates. Prior to functional measurements, the cells were incubated in the absence (−) or presence (+) of ponasterone A (*Pon A,* 10 μM) for an additional 24 h, followed by permeabilization of the plasma membrane with saponin (for details, see "Experimental Procedures"). The transport rates are normalized as a percentage of control values (−*Pon A*) measured in choline chloride-rich buffers (pH_o 7.8). *A*, prior to measurements of $^{22}Na^+$ influx (5 μCi of $^{22}NaCl$ (carrier-free)/ml), cells were untreated or pretreated with either the H^+ ionophore CCCP (2 μM) or the alkalizing agent NH_4Cl (30 mM) for 2 or 5 min, respectively, and were maintained during the 5-min uptake period. In one series of experiments, the NH_4Cl was rapidly washed out (+ *w/o*) of the cells prior to measurements of $^{22}Na^+$ influx in order to increase the acidity of the organellar compartments. *B*, initial rates of $^{22}Na^+$ influx were measured in the presence of amiloride (2 mM) or benzamil (0.1 and 1 mM). Values represent the average of 3–4 experiments, each performed in quadruplicate (mean ± S.D.). Differences in the experimental groups were analyzed by a one-way analysis of variance, and comparisons between means were carried out using the Newman-Keuls test at the 5% significance level (*asterisks* = $p < 0.05$).

nary experiments demonstrated that the sequestration of $^{22}Na^+$ in choline chloride-rich buffer was dependent on the external pH (*i.e.* maximal in more alkaline buffers) and linear over a 10-min period (data not shown); therefore, an external pH of 7.8 and a 5-min uptake period were chosen for the transport assay. As shown in Fig. 7*A*, $NHE7_{HA}$-expressing EcR-CHO cells had ~75% higher rates of $^{22}Na^+$ influx compared with uninduced cells. Since only ~50% of cells stably overexpress $NHE7_{HA}$ under these conditions, this percentage increase likely represents an underestimate of the actual cellular flux rates due to transfected $NHE7_{HA}$. Ponasterone A had no effect on untransfected EcR-CHO cells (data not shown). The role of pH was evaluated by treating cells with the H^+-specific ionophore carbonyl cyanide *m*-chlorophenylhydrazone (CCCP), which rapidly dissipates the organellar transmembrane H^+ gradient (17). As illustrated in Fig. 7*A*, 2 μM CCCP significantly reduced $^{22}Na^+$ influx in both uninduced and ponasterone A-treated cells when compared with controls. Likewise, alkalinization of endomembrane compartments by sustained exposure to 30 mM NH_4Cl, as previously described by Kim *et al.* (18), also led to decreased $^{22}Na^+$ influx. By contrast, pretreatment and rapid removal of NH_4Cl, which dramatically acidifies intracellular compartments due to the rapid efflux of ammonia (18), significantly elevated (~ 3-fold) $^{22}Na^+$ uptake in both uninduced and ponasterone A-induced cells. Taken together, these data indicate the existence of an endogenous organellar Na^+ influx pathway that depends on the transmembrane H^+ gradient and that is up-regulated in $NHE7_{HA}$-overexpressing cells.

We next tested whether the activity of $NHE7_{HA}$ was sensitive to amiloride derivatives that are known inhibitors of the NHEs and are relatively membrane-permeant. As shown in Fig. 7*B*, $^{22}Na^+$ influx was only weakly inhibited (~25%) by 2 mM amiloride, a concentration that is sufficient to abolish activity of the plasma membrane NHE1 isoform in CHO cells (46). $NHE7_{HA}$ was also insensitive to low concentrations (100 μM) of benzamil, an amiloride analogue, although it was blocked significantly at high concentrations (1 mM). Since 100 μM benzamil is known to block the Na^+-selective Na^+/H^+ exchanger in isolated mitochondria (47), the fluxes measured under our conditions are unlikely to include uptake into mitochondria, more so given that the mitochondrial matrix is alkaline under steady-state conditions.

To establish the cation selectivity of this pathway, we performed analogous uptake experiments using $^{86}Rb^+$, a radioactive congener of K^+. Unexpectedly, ponasterone A-induced $NHE7_{HA}$-expressing cells exhibited a similar increase (~75%) in the rate of $^{86}Rb^+$ influx compared with uninduced cells (Fig. 8*A*). This stimulation was not observed in untransfected EcR-CHO cells (data not shown) and, like $^{22}Na^+$ uptake, was inhibited by 2 μM CCCP and 1 mM benzamil. Increasing the concentration of external Na^+, K^+, or Li^+ substantially reduced $^{86}Rb^+$ transport in $NHE7_{HA}$-induced cells (Fig. 8*B*), suggesting that all these monovalent cations compete for binding to the same or

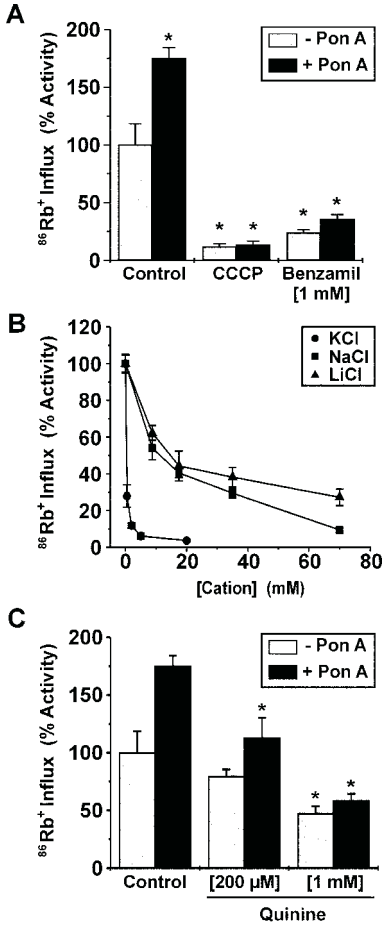

FIG. 8. **Measurements of H^+-dependent $^{86}Rb^+$ influx into endomembrane compartments of $NHE7_{HA}$-transfected EcR-CHO cells.** $NHE7_{HA}$-transfected EcR-CHO cells were grown to confluence in 24-well plates. Prior to functional measurements, the cells were incubated in the absence (−) or presence (+) of ponasterone A (*Pon A,* 10 μM) for an additional 24 h, followed by permeabilization of the plasma membrane with saponin (for details, see "Experimental Procedures"). The transport activities are normalized as a percentage of control values (− *Pon A*) measured in choline chloride-rich buffers (pH_o 7.8). *A*, initial rates of $^{86}Rb^+$ influx (5 μCi of $^{86}RbCl$ (carrier-free)/ml) were measured in the absence or presence of CCCP (2 μM) and benzamil (1 mM). *B*, initial rates of $^{86}Rb^+$ influx in ponasterone A-induced cells were measured in the presence of increasing concentrations of KCl (*closed circles*), NaCl (*closed squares*), and LiCl (*closed triangles*). Isoosmolarity was maintained by adjusting the choline chloride concentration. *C*, initial rates of $^{86}Rb^+$ influx were measured in the absence (control) or presence of increasing concentrations of quinine. Values represent the average of 3–4 experiments, each performed in quadruplicate (mean ± S.D.). Differences in the experimental groups were analyzed by a one-way analysis of variance, and comparisons between means were carried out using the Newman-Keuls test at the 5% significance level (*asterisks* = $p < 0.05$).

closely associated sites. By contrast, $^{86}Rb^+$ fluxes were relatively insensitive to divalent cations such as Zn^{2+} (200 μM) (Zn^{2+}-treated cells were 92.3 ± 10.7% of controls ($n = 4$); $p > 0.05$), which suggests that this pathway is distinct from the Zn^{2+}-inhibitable H^+ conductance recently identified in the Golgi complex (17). These data indicate that NHE7 functions as a nonselective monovalent cation/H^+ exchanger. Since K^+ is the main intracellular alkali cation, the physiologically relevant mode of transport is probably K^+/H^+ exchange. Thus, in addition to serving as a H^+ efflux pathway in the *trans*-Golgi network, NHE7 may also participate in controlling the luminal [K^+] which could influence volume homeostasis/morphology of this organelle.

The unique transport properties of NHE7 are particularly noteworthy in light of earlier biochemical studies that revealed the presence of two functionally distinct monovalent cation/proton exchangers in mammalian mitochondria. One of these preferentially mediates the exchange of matrix Na^+ for intermembrane H^+ generated by respiration (*i.e.* a Na^+-selective Na^+/H^+ exchanger) (48, 49) and is inhibited by benzamil derivatives of amiloride at micromolar concentrations (47, 50–52). It is constitutively active in respiring mitochondria and is primarily responsible for establishing the [Na^+] gradient ($[Na^+]_i < [Na^+]_o$) that allows Na^+-dependent extrusion of matrix Ca^{2+} (53). The other monovalent cation/H^+ exchanger is latent, transports all alkali cations (*i.e.* Li^+, Na^+, K^+, Rb^+, and Cs^+) at similar rates, is antagonized by drugs such as quinine, dicyclohexylcarbodiimide, and propranolol (54–56), and is postulated to play a role in organellar volume homeostasis (57). Again, since K^+ is the predominant intracellular alkali cation, it is simply referred to as a K^+/H^+ exchanger. At present, it is unclear which of the mammalian mitochondrial NHEs corresponds to the recently cloned mitochondrion-targeted NHE6 isoform since it has yet to be characterized functionally. However, in view of the high structural similarity between NHE7 and NHE6, we speculate that NHE6 may function as the mitochondrial quinine-sensitive K^+/H^+ exchanger. In this regard, we also find that $NHE7_{HA}$ activity is sensitive to inhibition by quinine (Fig. 8*C*), further suggestive of its functional similarity to one of the mitochondrial NHEs (*i.e.* NHE6). Further detailed pharmacological analyses are currently ongoing.

Homologues to human NHE6 and NHE7 have also been identified in lower eukaryotes, including the yeast *Saccharomyces cerevisiae* gene, *NHX1/NHA2* (24, 58), and the plant *Arabidopsis thaliana* gene, *AtNHX1* (59). Immunological analyses showed that yeast Nhx1 and plant AtNhx1 proteins localize predominantly to the late endosomal/prevacuolar and tonoplast/vacuolar compartments, respectively, and were capable of conferring tolerance to cytotoxic concentrations of NaCl (59–61). More recently, yeast Nhx1 was also found to be important for efficient protein trafficking out of the prevacuolar compartment (62). The latter results are particularly intriguing in view of the localization of NHE7 to the TGN and suggest that it may fulfill a similar physiological function. We are currently testing the hypothesis.

In summary, we describe the cloning and functional characterization of a novel monovalent cation/H^+ exchanger that localizes predominantly to the *trans*-Golgi network and likely plays an important role in maintaining the cation homeostasis and function of this important organelle.

Acknowledgments—We thank the following individuals for generously providing us with the reagents used in this study: J. Mort (Shriner's Hospital, Montreal, Canada) for the anti-cathepsin antibody; A. S. Verkman (University of California, San Francisco) for the mitochondrial and Golgi-GFP constructs; J. Bergeron (McGill University, Canada) for the anti-calnexin antibody; T. Hobman (University of Alberta, Canada) and M. G. Farquhar (University of California, San Diego) for the anti-α-mannosidase II antibodies; and J. S. Bonifacino (National Institutes of Health, Bethesda) for the CD25-TGN38 construct. We also thank H. Zaun and A. Boucher for technical assistance and J. Hanrahan for critically reading the manuscript.

REFERENCES

1. Saraste, M. (1999) *Science* **283,** 1488–1493
2. Garlid, K. D., Sun, X., Paucek, P., and Woldegiorgis, G. (1995) *Methods Enzymol.* **260,** 331–348
3. Brierley, G. P., Baysal, K., and Jung, D. W. (1994) *J. Bioenerg. Biomembr.* **26,** 519–526
4. Babcock, D. F., Herrington, J., Goodwin, P. C., Park, Y. B., and Hille, B. (1997) *J. Cell Biol.* **136,** 833–844
5. Mellman, I., Fuchs, R., and Helenius, A. (1986) *Annu. Rev. Biochem.* **55,** 663–700
6. Forgac, M. (1999) *J. Biol. Chem.* **274,** 12951–12954
7. van Weert, A. W. M., Dunn, K. W., Geuze, H. J., Maxfield, F. R., and Stoorvogel, W. (1995) *J. Cell Biol.* **130,** 821–834
8. Anderson, R. G., and Pathak, R. K. (1985) *Cell* **40,** 635–643
9. Mellman, I. (1992) *J. Exp. Biol.* **172,** 39–45

10. Puopolo, K., Kumamoto, C., Adachi, I., Magner, R., and Forgac, M. (1992) *J. Biol. Chem.* **267,** 3696–3706
11. Nishi, T., and Forgac, M. (2000) *J. Biol. Chem.* **275,** 6824–6830
12. Gluck, S. (1992) *J. Exp. Biol.* **172,** 29–37
13. Manolson, M. F., Wu, B., Proteau, D., Taillon, B. E., Roberts, B. T., Hoyt, M. A., and Jones, E. W. (1994) *J. Biol. Chem.* **269,** 14064–14074
14. Rybak, S. L., Lanni, F., and Murphy, R. F. (1997) *Biophys. J.* **73,** 674–687
15. Demaurex, N., Furuya, W., D'Souza, S., Bonifacino, J. S., and Grinstein, S. (1998) *J. Biol. Chem.* **273,** 2044–2051
16. Farinas, J., and Verkman, A. S. (1999) *J. Biol. Chem.* **274,** 7603–7606
17. Schapiro, F. B., and Grinstein, S. (2000) *J. Biol. Chem.* **275,** 21025–21032
18. Kim, J. H., Lingwood, C. A., Williams, D. B., Furuya, W., Manolson, M. F., and Grinstein, S. (1996) *J. Cell Biol.* **134,** 1387–1399
19. Frohman, M. A., Dush, M. K., and Martin, G. R. (1988) *Proc. Natl. Acad. Sci. U. S. A.* **85,** 8998–9002
20. Lubahn, D. B., Joseph, D. R., Sullivan, P. M., Willard, H. F., French, F. S., and Wilson, E. M. (1988) *Science* **240,** 327–330
21. Kozak, M. (1986) *Cell* **44,** 283–292
22. Humphrey, J. S., Peters, P. J., Yuan, L. C., and Bonifacino, J. S. (1993) *J. Cell Biol.* **120,** 1123–1135
23. Orlowski, J., and Grinstein, S. (1997) *J. Biol. Chem.* **272,** 22373–22376
24. Numata, M., Petrecca, K., Lake, N., and Orlowski, J. (1998) *J. Biol. Chem.* **273,** 6951–6959
25. Yun, C. H. C., Tse, C.-M., Nath, S. K., Levine, S. A., Brant, S. R., and Donowitz, M. (1995) *Am. J. Physiol.* **269,** G1–G11
26. Shrode, L. D., Gan, B. S., D'Souza, S. J., Orlowski, J., and Grinstein, S. (1998) *Am. J. Physiol.* **275,** C431–C439
27. Wakabayashi, S., Pang, T., Su, X., and Shigekawa, M. (2000) *J. Biol. Chem.* **275,** 7942–7949
28. Biemesderfer, D., DeGray, B., and Aronson, P. S. (1998) *J. Biol. Chem.* **273,** 12391–12396
29. Fafournoux, P., Noël, J., and Pouysségur, J. (1994) *J. Biol. Chem.* **269,** 2589–2596
30. Counillon, L., Pouysségur, J., and Reithmeier, R. A. F. (1994) *Biochemistry* **33,** 10463–10469
31. Tse, C.-M., Levine, S. A., Yun, C. H. C., Khurana, S., and Donowitz, M. (1994) *Biochemistry* **33,** 12954–12961
32. Biemesderfer, D., Pizzonia, J., Abu-Alfa, A., Exner, M., Reilly, R., Igarashi, P., and Aronson, P. S. (1993) *Am. J. Physiol.* **265,** F736–F742
33. Velasco, A., Hendricks, L., Moremen, K. W., Tulsiani, D. R., Touster, and Farquhar, M. G. (1993) *J. Cell Biol.* **122,** 39–51
34. Kneen, M., Farinas, J., Li, Y. X., and Verkman, A. S. (1998) *Biophys. J.* **74,** 1591–1599
35. Rotin, D., and Grinstein, S. (1989) *Am. J. Physiol.* **257,** C1158–C1165
36. Lippincott-Schwartz, J., Yuan, L. C., Bonifacino, J. S., and Klausner, R. D. (1989) *Cell* **56,** 801–813
37. Lippincott-Schwartz, J., Donaldson, J. G., Schweizer, A., Berger, E. G., Hauri, H. P., Yuan, L. C., and Klausner, R. D. (1990) *Cell* **60,** 821–836
38. Lippincott-Schwartz, J., Yuan, L., Tipper, C., Amherdt, M., Orci, L., and Klausner, R. D. (1991) *Cell* **67,** 601–616
39. Wood, S. A., Park, J. E., and Brown, W. J. (1991) *Cell* **67,** 591–600
40. Yang, W., and Storrie, B. (1998) *Mol. Biol. Cell* **9,** 191–207
41. D'Souza, S., Garcia-Cabado, A., Yu, F., Teter, K., Lukacs, G., Skorecki, K., Moore, H. P., Orlowski, J., and Grinstein, S. (1998) *J. Biol. Chem.* **273,** 2035–2043
42. Neupert, W. (1997) *Annu. Rev. Biochem.* **66,** 863–917
43. Schafer, W., Stroh, A., Berghofer, S., Seiler, J., Vey, M., Kruse, M. L., Kern, H. F., Klenk, H. D., and Garten, W. (1995) *EMBO J.* **14,** 2424–2435
44. Wong, S. H., and Hong, W. (1993) *J. Biol. Chem.* **268,** 22853–22862
45. Lin, P., Yao, Y., Hofmeister, R., Tsien, R. Y., and Farquhar, M. G. (1999) *J. Cell Biol.* **145,** 279–289
46. Counillon, L., and Pouysségur, J. (1993) *Biochim. Biophys. Acta* **1172,** 343–345
47. Brierley, G. P., Davis, M. H., Cragoe, E. J., Jr., and Jung, D. W. (1989) *Biochemistry* **28,** 4337–4354
48. Mitchell, P., and Moyle, J. (1969) *Eur. J. Biochem.* **9,** 149–155
49. Garlid, K. D., Shariat-Madar, Z., Nath, S., and Jezek, P. (1991) *J. Biol. Chem.* **266,** 6518–6523
50. Nath, S., and Garlid, K. D. (1988) in *Integration of Mitochondrial Function* (Lemasters, J. J., Hackenbrock, C. R., Thurman, R. G., and Westerhoff, H. V., eds) pp. 357–364, Plenum Publishing Corp., New York
51. Kapus, A., Lukacs, G. L., Cragoe, E. J., Jr., Ligeti, E., and Fonyó, A. (1988) *Biochim. Biophys. Acta* **944,** 383–390
52. Sastrasinh, M., Young, P., Cragoe, E. J., Jr., and Sastrasinh, S. (1995) *Am. J. Physiol.* **268,** C1227–C1234
53. Jung, D. W., Apel, L. M., and Brierley, G. P. (1992) *Am. J. Physiol.* **262,** C1047–C1055
54. Garlid, K. D. (1978) *Biochem. Biophys. Res. Commun.* **83,** 1450–1455
55. Martin, W. H., Beavis, A. D., and Garlid, K. D. (1984) *J. Biol. Chem.* **259,** 2062–2065
56. Brierley, G. P., Jurkowitz, M. S., Farooqui, T., and Jung, D. W. (1984) *J. Biol. Chem.* **259,** 14672–14678
57. DiResta, D. J., Kutschke, K. P., Hottois, M. D., and Garlid, K. D. (1986) *Am. J. Physiol.* **251,** R787–R793
58. Nass, R., Cunningham, K. W., and Rao, R. (1997) *J. Biol. Chem.* **272,** 26145–26152
59. Apse, M. P., Aharon, G. S., Snedden, W. A., and Blumwald, E. (1999) *Science* **285,** 1256–1258
60. Nass, R., and Rao, R. (1998) *J. Biol. Chem.* **273,** 21054–21060
61. Gaxiola, R. A., Rao, R., Sherman, A., Grisafi, P., Alper, S. L., and Fink, G. R. (1999) *Proc. Natl. Acad. Sci. U. S. A.* **96,** 1480–1485
62. Bowers, K., Levi, B. P., Patel, F. I., and Stevens, T. H. (2000) *Mol. Biol. Cell* **11,** 4277–4294
63. Kyte, J., and Doolittle, R. F. (1982) *J. Mol. Biol.* **157,** 105–132